A self-assembled, multicomponent water oxidation device†

Rita Tóth,[a] Roché M. Walliser,[b] Niamh S. Murray,[b] Debajeet K. Bora,[a] Artur Braun,[a] Guiseppino Fortunato,[c] Catherine E. Housecroft[b] and Edwin C. Constable*[b]

Langmuir–Blodgett (LB) and drop-cast (DC) films prepared from $[Ru(1)_3][PF_6]_2$ and Co_4POM (1 = 4,4′-bis(^{n}nonyl)-2,2′-bipyridine, $Co_4POM = K_{10}[Co_4(H_2O)_2(\alpha\text{-}PW_9O_{34})_2]$) have been evaluated as water oxidation catalysts and their electrocatalytic performances are reported; DC films evolve more O_2 per unit area than LB films and the catalyst is stable on an FTO surface for $\approx 500-600$ minutes.

Developing clean, renewable energy sources is one of the greatest challenges facing mankind,[1] and a promising approach is that of artificial photosynthesis.[2] Inspired by Nature and an understanding of the mechanisms exhibited by photosystems I and II many groups are investigating the photoelectrochemical or photocatalytic splitting of water into H_2 and O_2.[3] Of the two half-reactions of water splitting, oxidation to O_2 is more challenging involving four electrons, four protons, two H_2O molecules and the final formation of an O–O bond. High activation energies and slow kinetics motivates the development of water oxidation catalysts (WOC) which are efficient at minimal overpotential, hydrolytically and oxidatively stable and composed of inexpensive, earth-abundant materials.[4] Recently carbon-free, molecular polyoxometalate (POM) WOCs have been incorporated in both homogeneous and heterogeneous systems.[5] A polyoxometalate $K_{10}[Co_4(H_2O)_2(PW_9O_{34})_2]$ (Co_4POM) and a more efficient vanadium-containing polyoxometalate $[Co_4(H_2O)_2(VW_9O_{34})_2]^{10-}$, function as effective homogeneous WOCs when combined with an *in situ* generated $[Ru(bpy)_3]^{3+}$ oxidant.[6] A solid–aqueous interface,

can both control the organization of the components and enhance the overall efficacy.[7–12]

We have recently prepared films from $[Ru(1)_3][PF_6]_2$ (see Scheme 1 for ligand **1**) and Co_4POM on mica using the LB technique for use as a WOC in an electrochemical water splitting cell.[13] We now compare the electrocatalytic performance of LB layers with layer-by-layer drop-cast (DC) films of the same components on fluorine doped tin oxide (FTO) coated glass slides as a conductive substrate.

LB films were self-assembled on the substrates by the vertical lifting method, with withdrawal and immersion of the substrate through the film.[13] The substrate was allowed to dry in air after each withdrawal for 5 minutes prior to the next immersion/withdrawal cycle. The films were prepared with 50 dipping cycles. Details of the preparation of the LB and DC films are given in the ESI.†

SEM-FIB images of LB films before and after electrocatalytic treatment (Fig. S1 *versus* S2, ESI†) show that the surface of a multiple-layer LB film is smoother than the FTO surface (Fig. S3, ESI†) but is still rough. This surface structure of the electrodes is essential for the catalytic activity. The surface of the DC films is more uneven (Fig. S4, ESI†), with the film thickness ranging between 10 nm and a few microns.

To assess the WOC performances of the LB and DC films, along with films of the individual drop-cast components ($[Ru(1)_3][PF_6]_2$ and Co_4POM), cyclic voltammetry (CV) measurements were performed at pH 7.6 in phosphate buffer saline (PBS) solution in a three-electrode system (ESI†). Fig. 1 shows that the catalytic activity of the bare FTO-coated glass and the

[a] *Laboratory for High Performance Ceramics, Empa. Swiss Federal Laboratories for Materials Science and Technology, Uberlandstrasse 129, CH-8600, Dubendorf, Switzerland*

[b] *Department of Chemistry, University of Basel, Spitalstrasse 51, CH4056 Basel, Switzerland. E-mail: edwin.constable@unibas.ch*

[c] *Protection and Physiology, Empa, Swiss Federal Laboratories for Materials Science and Technology, Lerchenfeldstr. 5, 9014 St. Gallen, Switzerland*
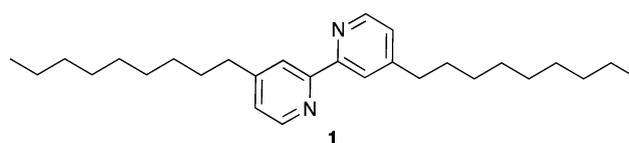
Scheme 1 Structure of ligand **1**. See Scheme S1 (ESI†) for the structure of $[Ru(1)_3]^{2+}$.

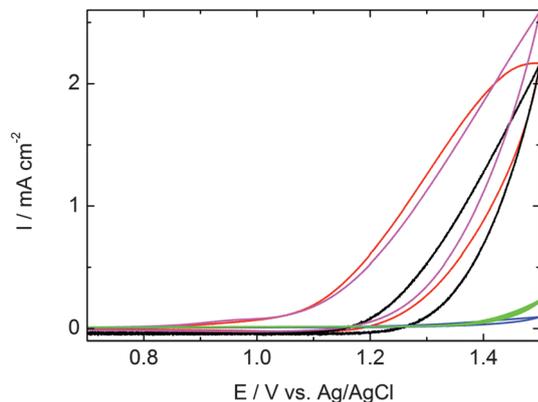**Fig. 1** CVs of 50-layer LB and DC films of $[Ru(\mathbf{1})_3][PF_6]_2/Co_4POM$ on FTO (black and red curves respectively), DC films of $[Ru(\mathbf{1})_3][PF_6]_2$ (blue) and Co_4POM (magenta) on FTO, and bare FTO (green). Scan rate: 25 mV s^{-1}. Complete CVs are shown in Fig. S5 (ESI†).

$[Ru(\mathbf{1})_3][PF_6]_2$ drop cast film is negligible. In contrast, the Co_4POM drop cast film exhibited larger current density than the LB and DC combined WOC ($[Ru(\mathbf{1})_3]^{2+}/Co_4POM$) films. The onset of catalytic current of the DC film and Co_4POM films occurs at nearly the same potential (+1.11 V and +1.13 V vs. Ag/AgCl, respectively), however, the current onsets at ~0.1 V higher potential (+1.23 V vs. Ag/AgCl) in the case of LB films. The overpotential is at least 0.52 V over the thermodynamic potential for water oxidation at pH 7.6 (0.59 V vs. Ag/AgCl). The current density of 2.16 mA cm^{-2} is associated with the catalytic action of the combined $[Ru(\mathbf{1})_3][PF_6]_2/Co_4POM$ system.

To monitor the amount of O_2 evolved from the reaction between the $[Ru(\mathbf{1})_3][PF_6]_2/Co_4POM$ system and H_2O we have developed a closed cycle, recirculating gas chromatography (GC) system equipped with a custom-built, sealed electrochemical cell (Fig. S6, ESI†). A long term (over 1000 minutes) electrolysis was carried out by applying a constant potential of +1.3 V vs. Ag/AgCl (and +1.0 V vs. Ag/AgCl, see Fig. S7, ESI†) in PBS electrolyte. Sustainable O_2 evolution was observed for ≈600 min for all four types of film, indicating the stability of the catalyst system on the FTO surface for a relative long time (Fig. 2). Although no further oxygen evolution was detected after 600 minutes from
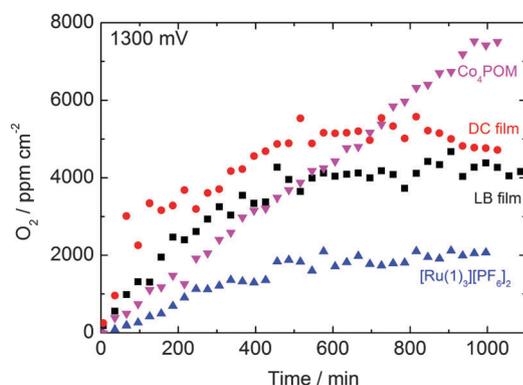
the LB and DC films or $[Ru(\mathbf{1})_3][PF_6]_2$, the oxygen amount in the headspace steadily increased during the 1100 minutes for which the reaction was monitored above the Co_4POM film. The DC films evolved slightly more O_2 per area than the LB films. However, the thickness of the DC films is greater and the surface was more uneven than the layers prepared by the LB technique (Fig. S4 and S8, ESI†).

Under a lower applied bias of +1 V vs. Ag/AgCl the DC, Co_4POM and $[Ru(\mathbf{1})_3][PF_6]_2$ films evolve approximately the same amount of O_2 as at +1.3 V vs. Ag/AgCl bias (Fig. S7, ESI†) since the applied potentials are higher than their water oxidation onset potential. The LB film performs better at +1.3 V than at +1.0 V bias potential due to its higher onset potential of +1.23 V (Fig. S7, ESI†).

The long-term stability of the systems was confirmed by chronoamperometric measurements. A bias of +1.3 V (vs. Ag/AgCl) was applied for >600 minutes and the current was recorded under working conditions (Fig. 3). After the initial drop, the current was relatively stable. The spikes on the curves are due to bubble formation on, and desorption from the surface of the film. The results are similar to those for a study related to a spinel mixed oxide electrode.[14] On the smoother surface of the LB films, fewer bubbles form than on the rough surface of the DC films. The height of the spikes scales with the observed current density.

We compared the amount of evolved O_2 measured by gas chromatography with the theoretical number of moles of O_2 obtained from the current density data (shown in Fig. 3) applying Faraday's law (integrated current/4F) (Fig. 4).[15] The amount of O_2 determined from the GC experiment is around six times lower than that calculated for DC films and about one third of the theoretical value for LB films at 600 minutes. This can be attributed to the dissolution of O_2 in the relatively large volume of electrolyte (59 cm^3) compared to the 1 cm^2 area of the electrode containing ~3.5 nmol catalyst. The measured current density may also include parasitic side reactions. It is evident that the amount of catalyst material on the FTO substrate is lower after anodizing the electrodes for a significant period of time than in the initial DC and LB films (Fig. S8, ESI†). Initially, the electrodes show structures with a cracked pattern similar

Fig. 2 O_2 evolution vs. time at +1.3 V bias for LB and DC films prepared from $[Ru(\mathbf{1})_3][PF_6]_2$ and Co_4POM, and separate DC Co_4POM and $[Ru(\mathbf{1})_3][PF_6]_2$ films.
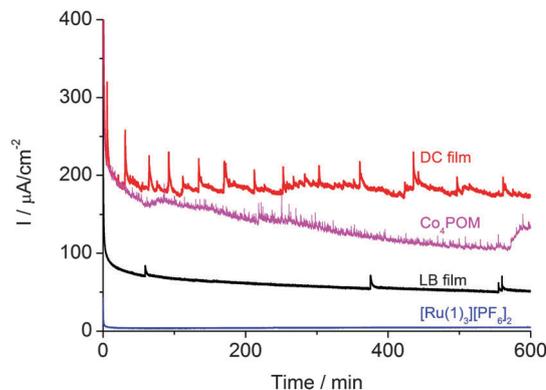

Fig. 3 Current densities of LB and DC films, and DC Co_4POM and $[Ru(\mathbf{1})_3][PF_6]_2$ films during chronoamperometry (+1.3 V bias vs. Ag/AgCl). Spikes are caused by surface bubble formation.
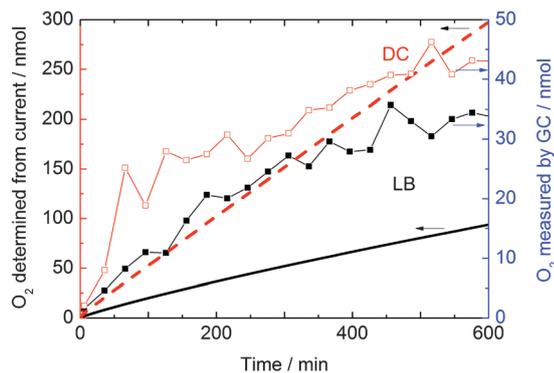
Fig. 4 Comparison of the evolved O_2 from the LB and DC films measured by GC and calculated from the current density data using Faraday's law. The red open symbols are from the DC films. The black filled symbols are from the LB films. The symbols present measured gas amounts (right axis). The dashed red line and the solid black line are the integrated current over time divided by four times the Faraday constant from the DC and LB films, respectively (left axis).

to the Co–Pi catalyst surface reported by Nocera.[7] The post-electrochemical treated films show a very small amount of catalyst and the bare FTO surface is clearly visible in scanning electron microscopy (SEM) images (Fig. S8, ESI†) taken after 1000 min operation. However, the film thickness and surface structure remained the same after, (Fig. S1 and S2, ESI†), and the films were stable during, 1 h of catalytic activity.

The estimated amounts of Co_4POM and $[Ru(\mathbf{1})_3][PF_6]_2$ in the LB film are ≤ 3.5 nmol cm^{-2} and ≤ 1.5 nmol cm^{-2}, respectively, and 1370 nmol cm^{-2} for the complexes in the DC film. From 1 cm^2 LB and DC films, 34 and 43 nmol O_2 evolved, respectively, in 600 minutes as measured by gas chromatography. The theoretical values for the same time interval, which were calculated from the current density data, are 94 and 298 nmol for 1 cm^2 LB and DC films. Both measured and calculated values far exceed the amount that the stoichiometric reaction with water would give. The calculated turnover numbers and turnover frequencies for the LB and DC films are the following: TON = $n_{O_2}/n_{catalyst}$ = 23 mol O_2 per mol $[Ru(\mathbf{1})_3][PF_6]_2$ or 10 mol O_2 per mol Co_4POM in 600 min for 1 cm^2 LB films, and 0.03 mol O_2 per mol complex on 1 cm^2 DC films; TOF = $n_{O_2}/n_{catalyst}$ = 0.0006 mol O_2 per s per mol $[Ru(\mathbf{1})_3][PF_6]_2$ or 0.00028 mol O_2 per s per mol Co_4POM for 1 cm^2 LB films, and 0.00005 mol O_2 per s per mol complex on 1 cm^2 DC films. The TOF is lower than the value reported[6] for a similar WOC system used as a homogeneous catalyst (≥ 5 s^{-1}). In contrast to homogeneous catalysis where all molecules contribute to the catalytic activity, heterogeneous catalysis only occurs at selected surface sites. This is a likely reason for the lower TOF. Our TOF value is comparable to that of 0.0007 s^{-1} calculated for the WOC formed *in situ* on the surface of an indium tin oxide electrode from Co^{2+} containing neutral aqueous phosphate solution.[7] Although a TOF value was not reported in Nocera's[7] work, it was possible to calculate[9] the lower limit since the amount of catalyst was given.

Powders and films of $[Ru(\mathbf{1})_3][PF_6]_2$ and Co_4POM were studied by X-ray diffraction (XRD) to examine how they changed

during film preparation. It is clear that the $[Ru(\mathbf{1})_3][PF_6]_2$ powder and film contain ruthenium(III) metaphosphate, $Ru(PO_3)_3$, which has a triclinic structure and is built from Ru^{3+} ions and infinite $[PO_3^-]_\infty$ chains.[16] The Co_4POM powder and film contain $K_2CoWO_2(PO_4)_2$, which is a possible building block of the $[Co_4(H_2O)_2(PW_9O_{34})_2]^{10-}$ polyoxometalate. Interestingly, in the DC film of the mixture of $[Ru(\mathbf{1})_3][PF_6]_2$ and Co_4POM, a third kind of peak appears which is a convolution of the $Ru(PO_3)_3$ and $K_2CoWO_2(PO_4)_2$ peaks. This suggests an interaction between the ruthenium complex and Co_4POM occurs during film preparation. The XRD results also reveal the presence of $CoO_{1.29}$ both in the DC and LB films. The XRD patterns of the films before and after electrocatalytic activity were also compared. Similar to the SEM images, the XRD results confirm the desorption of most of the films from the substrate during 1000 minutes catalytic activity. The occurrence of Co2p, W4f, Ru3p and N1s peaks in X-ray photoelectron spectroscopy (XPS) survey scans confirm the presence of both Co_4POM and $[Ru(\mathbf{1})_3][PF_6]_2$ in the films. For detailed XRD and XPS analysis see Fig. S9–S13 and Table S1 (ESI†) and accompanying text.

The DC films evolve about 10 nmol cm^{-2} more O_2 than the LB films at +1.3 V applied bias potential. The onset potential for DC $[Ru(\mathbf{1})_3][PF_6]_2/Co_4POM$ and DC Co_4POM films is ≈ 0.1 V lower than for the LB $[Ru(\mathbf{1})_3][PF_6]_2/Co_4POM$ films, possibly arising from the larger surface area with more catalytic sites on the island-like structure of the DC film shown on the SEM images (Fig. S8, ESI†). Although the Co_4POM evolves less O_2 during the first 500–700 minutes than the LB and DC $[Ru(\mathbf{1})_3][PF_6]_2/Co_4POM$ system, it continues to produce a linearly increasing amount of O_2 after the other two films have reached saturation. As significantly less Co_4POM was observed on the electrode after electrolysis than before electrolysis, it appears that Co_4POM worked in part as a homogeneous catalyst and also partially decomposed to CoO_x, which is an effective WOC catalyst. An ongoing debate concerns the stability of Co_4POM and whether the polyoxometalate or CoO_x is the true catalyst in the homogeneous systems. The reaction conditions, (pH, bias potential, buffer and the concentration of the catalyst) have a huge impact on the stability of Co_4POM.[17] In the homogeneous system, not only water molecules but also the organic ligand of the Ru complex are oxidized, furthermore precipitates form from the Co_4POM and Ru complex and Co_4POM decomposes in phosphate buffer at neutral and basic pH values where the POM catalyst is most active. When the catalyst is immobilized on an electrode surface, desorption of the catalyst and oxidant/photosensitizer is also an issue.[18] All of these parameters affect the stability of our catalytic system and contribute to the cessation of catalytic activity after 600 minutes. The detailed investigation of the stability of the system was not the scope of this study.

In conclusion, we have prepared two kinds of water oxidizing electrodes: (i) alternating, smooth Langmuir–Blodgett monolayers of abundant, inorganic Co_4POM catalyst and $[Ru(\mathbf{1})_3][PF_6]_2$ oxidant and (ii) also alternating, uneven drop cast layers of the two above mentioned components, both on FTO substrate. We have found that both electrodes are efficient oxygen evolving anodes at pH 8 and the DC film evolves slightly more O_2 per geometrical area due

to its higher surface area. The catalyst is stable on the FTO surface for about 500–600 minutes. In long term operation, the drop cast Co_4POM catalyst on its own evolves more O_2 than the $[Ru(1)_3][PF_6]_2/Co_4POM$ combined layers, most likely because it is not stable on the FTO surface and works as a homogeneous catalyst in the electrolyte. The turnover frequency of the LB and DC electrodes is lower than that of the homogeneous system of the same components reported by Hill,[6] however, it is higher than the turnover frequency reported for Co_4POM forming *in situ* on the surface of indium tin oxide electrode.[7] Potentially, the stability of the system could be enhanced in the future by improving the binding of the catalyst system to the substrate and the components to each other, avoiding phosphate buffer and using for example borate buffer and using as low as possible bias potential. Organic oxidant/photosensitiser should also be avoided but a viable inorganic component has not yet been developed.

Notes and references

1 J. Chow, R. J. Kopp and P. R. Portney, *Science*, 2003, **302**, 1528.
2 K. Arifin, E. H. Majlan, W. R. W. Daud and M. B. Kassim, *Int. J. Hydrogen Energy*, 2012, **37**, 3066; L. Duan, F. Bozoglian, S. Mandal, B. Stewart, T. Privalov, A. Llobet and L. Sun, *Nat. Chem.*, 2012, **4**, 418; A. Thapper, S. Styring, G. Saracco, A. W. Rutherford, B. Robert, A. Magnuson, W. Lubitz, A. Llobet, P. Kurz, A. Holzwarth, S. Fiechter, H. de Groot, S. Campagna, A. Braun, H. Bercegol and V. Artero, *Green*, 2013, **3**, 43.
3 See for example: J. G. McAlpin, T. A. Stich, W. H. Casey and R. D. Britt, *Coord. Chem. Rev.*, 2012, **256**, 2445; X. Liu and F. Wang, *Coord. Chem. Rev.*, 2012, **256**, 1115; G. Wang, Y. Ling, H. Wang, L. Xihong and Y. Li, *J. Photochem. Photobiol., C*, 2014, **19**, 35; V. Balzani, A. Credi and M. Venturi, *ChemSusChem*, 2008, **1**, 26.
4 H. Yamazaki, A. Shouji, M. Kajita and M. Yagi, *Coord. Chem. Rev.*, 2010, **254**, 2483; M. Yagi, A. Syouji, S. Yamada, M. Komi, H. Yamazaki and S. Tajima, *Photochem. Photobiol. Sci.*, 2009, **8**, 139.
5 H. Lv, Y. V. Geletii, C. Zhao, J. W. Vickers, G. Zhu, Z. Luo, J. Song, T. Lian, D. G. Musaev and C. L. Hill, *Chem. Soc. Rev.*, 2012, **41**, 7572.
6 Q. Yin, J. M. Tan, C. Besson, Y. V. Geletii, D. G. Musaev, A. E. Kuznetsov, Z. Luo, K. I. Hardcastle and C. L. Hill, *Science*, 2010, **328**, 342; H. Lv, J. Song, Y. V. Geletii, J. W. Vickers, J. M. Sumliner, D. G. Musaev, P. Kögerler, P. F. Zhuk, J. Bacsa, G. Zhu and C. L. Hill, *J. Am. Chem. Soc.*, 2014, **136**, 9268.
7 M. W. Kanan and D. G. Nocera, *Science*, 2008, **321**, 1072.
8 W. J. Youngblood, S.-H. A. Lee, Y. Kobayashi, E. A. Hernandez-Pagan, P. G. Hoertz, T. A. Moore, A. L. Moore, D. Gust and T. E. Mallouk, *J. Am. Chem. Soc.*, 2009, **131**, 926; P. K. Ghosh, B. S. Brunschwig, M. Chou, C. Creutz and N. Sutin, *J. Am. Chem. Soc.*, 1984, **106**, 4772; I. A. Weinstock, E. M. G. Barbuzzi, M. W. Wemple, J. J. Cowan, R. S. Reiner, D. M. Sonnen, R. A. Heintz, J. S. Bond and C. L. Hill, *Nature*, 2001, **414**, 191.
9 F. Jiao and H. Frei, *Angew. Chem., Int. Ed.*, 2009, **48**, 1841.
10 G. Sprintschnik, H. W. Sprintschnik, P. P. Kirsch and D. G. Whitten, *J. Am. Chem. Soc.*, 1977, **99**, 4947.
11 G. L. Gaines, Jr, P. E. Behnken and S. J. Valenty, *J. Am. Chem. Soc.*, 1978, **100**, 6549.
12 J. Wu, L. Liao, W. Yan, Y. Xue, Y. Sun, X. Yan, Y. Chen and Y. Xie, *ChemSusChem*, 2012, **5**, 1207; X. Xiang, J. Fielden, W. Rodríguez-Cordoba, Z. Huang, N. Zhang, Z. Luo, D. G. Musaev, T. Lian and C. L. Hill, *J. Phys. Chem. C*, 2013, **117**, 918; F. M. Toma, A. Sartorel, M. Iurlo, M. Carraro, P. Parisse, C. Maccato, S. Rapino, B. R. Gonzalez, H. Amenitsch, T. Da Ros, L. Casalis, A. Goldoni, M. Marcaccio, G. Scorrano, G. Scoles, F. Paolucci, M. Prato and M. Bonchio, *Nat. Chem.*, 2010, **2**, 826; N. Anwar, A. Sartorel, M. Yaqub, K. Wearen, F. Laffir, G. Armstrong, C. Dickinson, M. Bonchio and T. McCormac, *ACS Appl. Mater. Interfaces*, 2014, **6**, 8022; S. M. Lauinger, J. M. Sumliner, Q. Yin, Z. Xu, G. Liang, E. N. Glass, T. Lian and C. L. Hill, *Chem. Mater.*, 2015, **2**, 5886; J. Fielden, J. M. Sumliner, N. Han, Y. V. Geletii, X. Xiang, D. G. Musaev, T. Lian and C. L. Hill, *Chem. Sci.*, 2015, **6**, 5531; M. Nagai, H. Sanpei and M. Shirakura, *J. Mater. Chem.*, 2012, **22**, 9222.
13 N. S. Murray, J. A. Rudd, A.-C. Chamayou, E. C. Constable, C. E. Housecroft, M. Neuburger and J. A. Zampese, *RSC Adv.*, 2014, **4**, 11766.
14 T. Maiyalagan, K. A. Jarvis, S. Therese, P. J. Ferreira and A. Manthiram, *Nat. Commun.*, 2014, **5**, 3949.
15 D. K. Bora, A. Braun, R. Erni, G. Fortunato, T. Graule and E. C. Constable, *Chem. Mater.*, 2011, **23**, 2051.
16 H. Fukuoka, H. Imoto and T. Saito, *J. Solid State Chem.*, 1995, **119**, 107.
17 See for example: J. J. Stracke and R. G. Finke, *J. Am. Chem. Soc.*, 2011, **133**, 14872; M. Natali, S. Berardi, A. Sartorel, M. Bonchio, S. Campagna and F. Scandola, *Chem. Commun.*, 2012, **48**, 8808; J. J. Stracke and R. G. Finke, *ACS Catal.*, 2013, **3**, 1209; J. W. Vickers, H. Lv, J. M. Sumliner, G. Zhu, Z. Luo, D. G. Musaev, Y. V. Geletii and C. L. Hill, *J. Am. Chem. Soc.*, 2013, **135**, 14110; J. J. Stracke and R. G. Finke, *ACS Catal.*, 2014, **4**, 79.
18 J. M. Sumliner, H. Lv, J. Fielden, Y. V. Geletii and C. L. Hill, *Eur. J. Inorg. Chem.*, 2014, 635.